

# Viscoelastic-plastic Material Models: a Comparison Between Numerical Results and Experimental Tests

**Bruno Crisman**

Department of Engineering and Architecture  
University of Trieste, P.le Europa 1  
34127 Trieste, Italy

**Alfonso Nappi**

Department of Engineering and Architecture  
University of Trieste, P.le Europa 1  
34127 Trieste, Italy

**Abstract**—A *viscoelastic-plastic material model* applicable to three-dimensional stress states has been considered as a viable alternative to describe the behavior of structural systems made of *bituminous mixtures* in a relatively simple way. Actually, this model, which takes into account both *viscous* and *plastic* strains, appears to be suitable for the numerical analysis of systems subjected to time-dependent loads of different nature, although it requires a limited number of parameters and can be implemented in traditional, robust algorithms developed for nonlinear materials.

In this paper, we will make use of finite element meshes and, for each sample problem, will carry out an incremental analysis in order to compute the time-dependent viscous strains. To this aim, we will subdivide the load history into a finite number of time-steps. In addition, since the material model also includes plastic deformations, the computer code will exploit an iterative algorithm to determine the non-reversible strains during each time-step.

The numerical examples will focus on the response of cylindrical test specimens subjected to compression loads, with special emphasis given to *square-wave loading*. However, *static creep tests* will also be considered, in order to check the response of the *viscoelastic-plastic material model* in the presence of different load conditions. More specifically, we will compare numerical results with experimental data, showing that a convenient choice of seven parameters can lead to accurate results in very different situations, even though the material model is relatively simple and can easily fit in any computer program designed for nonlinear structural analysis.

**Keywords**—*bituminous mixtures; deviatoric and isotropic stress/strain components; discrete numerical models; finite element method; repeated load axial tests; square-wave loading; static creep tests; structural analysis; viscoelastic-plastic materials; Voigt model*

## I. INTRODUCTION

*Viscoelastic-plastic materials* have been the topic of research activities for several decades [1-5], but

apparently their use in the analysis of pavements has been quite limited, even if today's computational tools can easily deal with nonlinear problems.

Essentially, this paper is part of a preliminary study on the three-dimensional analysis of *viscoelastic-plastic* systems by using a material model, which is suitable to describe the response of *bituminous mixtures* and was discussed in a previous work [6].

On that occasion, we checked the performance of an algorithm for the estimate of parameters through the numerical simulation of *static creep tests* (*i.e.*, by considering fictitious measurements and by adjusting some parameters in order to define a discrete model whose response was as close as possible to the experimental data).

Here, instead, we will mostly focus on the performance of the same material model, when a *repeated square-wave compression load* is applied to a test specimen, with the aim of checking whether a relatively simple model can be considered for the structural analysis of pavements subjected to a variety of load conditions.

As anticipated in the previous paragraph, the model we are talking about is quite simple (nonlinear, but characterized by only seven parameters) and assumes a macroscopically homogeneous, isotropic material. In consequence, we cannot expect extremely accurate results in the presence of any load condition, but some comparisons with experimental results suggest that the overall response of *bituminous mixtures* can be determined with a good degree of accuracy. Indeed, viscoplastic strains provide useful information about the time-dependent response of structural systems. On the contrary, it would be clearly impossible to describe the effects due to persistent loads or recovery or alternating loads by performing an elastic analysis [7-9], as typically happens when a *complex modulus* or *resilient modulus* is estimated with the aim of introducing an average/equivalent elastic stiffness parameter.

In addition, *viscoelastic-plastic material models* can simulate the permanent deformation of pavements (*rutting*) caused by repeated loads, since non-reversible strains are taken into account. More in general, they can be used to study the response to quasi-static loads, load pulses (with convenient rest

periods), sinusoidal external forces and time-dependent loads of any type.

In the next Sections, we will compare numerical results with the experimental data related to a specimen subjected to *repeated compression loads with a square-wave pattern*. It will be shown that the actual response can be approximated with excellent accuracy. Perhaps more importantly, it will also be shown that it is possible to reach a *compromise solution*, which allows us to obtain satisfactory results in the presence of *repeated loads* and *static creep tests* as well, by selecting convenient values for the governing parameters.

Therefore, it seems to be reasonable to assume that even a simple *viscoelastic-plastic material model* could be considered, whenever we are interested in a realistic analysis of pavements subjected to time-dependent loads, which cannot be performed by using elastic models.

## II. A VISCOELASTIC-PLASTIC MATERIAL MODEL

Here, we will give some general information about the *viscoelastic-plastic material model*, which will be used for the numerical tests. Further details can be found in a previous publication [6].

By assuming a macroscopically homogeneous, isotropic material, when viscous and plastic strains are considered, the stress vector can be defined as follows:

$$\begin{aligned} \boldsymbol{\sigma} &= \boldsymbol{\sigma}_m + \mathbf{s} = 3 K \{ \boldsymbol{\varepsilon}_m - \boldsymbol{\varepsilon}_m^P \} + 2 G \{ \mathbf{e} - \mathbf{e}^P \} = \\ &= 3 K^* \boldsymbol{\xi}_m + 2 G^* \mathbf{d} + 3 \eta_V \dot{\boldsymbol{\xi}}_m + 2 \eta_D \dot{\mathbf{d}} \end{aligned} \quad (1)$$

where  $\boldsymbol{\sigma}$  and  $\boldsymbol{\sigma}_m$  represent vectors of stresses and mean stresses, while  $\boldsymbol{\varepsilon}_m$  and  $\boldsymbol{\varepsilon}_m^P$  are vectors, which depend upon the volumetric strains  $\varepsilon_v$  and plastic volumetric strains  $\varepsilon_v^P$ , such that  $\boldsymbol{\sigma}_m = 3K\{\boldsymbol{\varepsilon}_m - \boldsymbol{\varepsilon}_m^P\}$ , if  $K$  denotes the *bulk modulus*.

Similarly,  $\mathbf{s}$ ,  $\mathbf{e}$  and  $\mathbf{e}^P$  represent vectors of deviatoric stresses, deviatoric strain and deviatoric plastic strains such that  $\mathbf{s} = 2G\{\mathbf{e} - \mathbf{e}^P\}$ , if  $G$  denotes the *shear modulus*. As for  $\boldsymbol{\xi}_m$ ,  $\mathbf{d}$ ,  $K^*$  and  $G^*$ , these quantities are fully analogous to  $\boldsymbol{\varepsilon}_m$ ,  $\mathbf{e}$ ,  $K$  and  $G$ , but are concerned with *viscous strains*. In addition,  $\eta_V$  and  $\eta_D$  are *viscous coefficients*, which govern the contribution to the stress vector given by the strain rates  $\dot{\boldsymbol{\xi}}_m$  and  $\dot{\mathbf{d}}$ .

As usual, the stress and strain vectors will only include independent components. Therefore, after introducing the *mean stress*  $\sigma_m = (\sigma_{11} + \sigma_{22} + \sigma_{33})/3$ , we have implicitly assumed the vectors  $\boldsymbol{\sigma} = [\sigma_{11} \ \sigma_{22} \ \sigma_{33} \ \sigma_{12} \ \sigma_{23} \ \sigma_{31}]^T$ ,  $\boldsymbol{\sigma}_m = [\sigma_m \ \sigma_m \ \sigma_m \ 0 \ 0 \ 0]^T$  and  $\mathbf{s} = [s_{11} \ s_{22} \ s_{33} \ s_{12} \ s_{23} \ s_{31}]^T$ , as well as  $\boldsymbol{\varepsilon}_m = [\varepsilon_v/3 \ \varepsilon_v/3 \ \varepsilon_v/3 \ 0 \ 0 \ 0]^T$  and  $\mathbf{e} = [e_{11} \ e_{22} \ e_{33} \ e_{12} \ e_{23} \ e_{31}]^T$ . Of course, the vectors  $\boldsymbol{\varepsilon}_m^P$  and  $\boldsymbol{\xi}_m$  are analogous to  $\boldsymbol{\varepsilon}_m$ , while  $\mathbf{e}^P$  and  $\mathbf{d}$  are analogous to  $\mathbf{e}$ .

Since we shall need a few key relationships when we introduce finite element models, it is convenient to remind that an infinitesimal contribution to the strain energy per unit volume is given by  $\sigma_{ij}(d\varepsilon_{ij} - d\varepsilon_{ij}^P)$  or, alternatively,  $\sigma_m(d\varepsilon_v - d\varepsilon_v^P) + s_{ij}(de_{ij} - de_{ij}^P)$  (with  $i$  and  $j$

ranging between 1 and 3). In consequence, keeping in mind how the vectors  $\boldsymbol{\sigma}_m$ ,  $\mathbf{s}$ ,  $\boldsymbol{\varepsilon}_m$ ,  $\boldsymbol{\varepsilon}_m^P$ ,  $\mathbf{e}$  and  $\mathbf{e}^P$  have been defined, we shall set  $\sigma_m(d\varepsilon_v - d\varepsilon_v^P) = \boldsymbol{\sigma}_m^T \{d\boldsymbol{\varepsilon}_m - d\boldsymbol{\varepsilon}_m^P\}$  for the isotropic components and  $s_{ij}(de_{ij} - de_{ij}^P) = \mathbf{s}^T \mathbf{M} \{d\mathbf{e} - d\mathbf{e}^P\}$  for the deviatoric components, where  $\mathbf{M}$  is a diagonal matrix, whose significant entries are  $M_{11} = M_{22} = M_{33} = 1$  and  $M_{44} = M_{55} = M_{66} = 2$ .

It may also be of some interest to observe that eqns. (1), rewritten in a simplified way, would represent the governing equations for the mechanical model, which is shown in Fig. 1 and is concerned with a uniaxial stress state. Indeed, we can set

$$Q = k(u - u^P) = g u_V + h \dot{u}_V \quad (2)$$

Here,  $u$  refers to the relative displacement between the points A and B,  $u^P$  represents the non-reversible relative displacement that may occur in the element identified by a black square in Fig. 1 (element that is subjected to possible plastic strains) and  $u_V$  denotes viscous displacements. In addition,  $k$  and  $g$  are the *stiffness parameters* of the linear elastic springs, while  $h$  is a *viscous coefficient*.

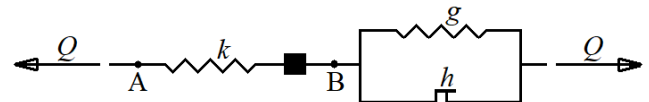


Fig. 1. Mechanical model for the viscoelastic-plastic material.

Eqn. (2) can also be written in terms of stresses and strains by introducing the *elastic moduli*  $E$  and  $E^*$ , together with a convenient *viscous coefficient*  $\eta$  and the relevant viscous strains  $\varepsilon^*$ :

$$\sigma = E(\varepsilon - \varepsilon^P) = E^* \varepsilon^* + \eta \dot{\varepsilon}^* \quad (3)$$

It might also be interesting to observe that the *viscous damper* in parallel with a spring (on the right hand side of the schematic representation in Fig. 1) is typical of the classical *Kelvin-Voigt model* or *Voigt model*, which can be used to describe the behavior of *viscoelastic systems*.

In order to use the material model discussed above in the framework of a finite element analysis, we can apply the principle of virtual displacements to each element.

By following this approach, we need to compute some integrals concerned with the volume of every element and its surface (when a portion of an element belongs to the external surface of the discretized body). Thus, by observing that the scalar product between isotropic and deviatoric quantities is zero, we obtain

$$\begin{aligned} & \int \{ \boldsymbol{\sigma}_m + \mathbf{s} \}^T \{ \delta \boldsymbol{\varepsilon}_m + \mathbf{M} \delta \mathbf{e} \} dV = \\ &= \int 3K \{ \boldsymbol{\varepsilon}_m - \boldsymbol{\varepsilon}_m^P \}^T \delta \boldsymbol{\varepsilon}_m dV + \int 2G \{ \mathbf{e} - \mathbf{e}^P \}^T \mathbf{M} \delta \mathbf{e} dV = \\ &= \int \mathbf{b}^T \delta \mathbf{u} dV + \int \mathbf{f}^T \delta \mathbf{u} dS \end{aligned} \quad (4)$$

Here, the vectors  $\mathbf{b}$  and  $\mathbf{f}$  refer to body forces and surface forces, while  $\mathbf{u}$  denotes the displacements due to the reversible and non-reversible (plastic) strains.

Then, by introducing a matrix of shape functions  $\Phi$ , we can set (for each element)  $\mathbf{u}=\Phi \mathbf{u}_N$ , where  $\mathbf{u}_N$  collects the nodal displacements compatible with the reversible and non-reversible strains.

Similarly, we can set  $\boldsymbol{\varepsilon}_m=\mathbf{B}_V \mathbf{u}_N$  and  $\mathbf{e}=\mathbf{B}_D \mathbf{u}_N$ , if the matrices  $\mathbf{B}_V$  and  $\mathbf{B}_D$  collect convenient derivatives of the shape functions.

As for the plastic strains, we can consider (for each element) a convenient number of *strain points*, where the isotropic components  $\boldsymbol{\varepsilon}_m^P$  and the deviatoric components  $\mathbf{e}^P$  are defined. Such points are usually inside the element and can coincide with the points used for the numerical integration (e.g., *Gauss points* in the case of quadrilateral or hexahedral elements). If the values attained by  $\boldsymbol{\varepsilon}_m^P$  and  $\mathbf{e}^P$  at the *strain points* are collected into the vectors  $\boldsymbol{\lambda}_e$  and  $\boldsymbol{\mu}_e$ , it is possible to introduce the relationships  $\boldsymbol{\varepsilon}_m^P=\Phi_P \boldsymbol{\lambda}_e$  and  $\mathbf{e}^P=\Phi_P \boldsymbol{\mu}_e$ , where  $\Phi_P$  is another matrix of shape functions.

At this stage, we obtain

$$\begin{aligned} \int\left\{\boldsymbol{\sigma}_m+\mathbf{s}\right\}^T\left\{\delta \boldsymbol{\varepsilon}_m+\mathbf{M} \delta \mathbf{e}\right\} d V & =\delta \mathbf{u}_N^T\left[\int 3 K \mathbf{B}_V^T \mathbf{B}_V d V\right] \mathbf{u}_N+ \\ & +\delta \mathbf{u}_N^T\left[\int 2 G \mathbf{B}_D^T \mathbf{M} \mathbf{B}_D d V\right] \mathbf{u}_N+ \quad (5a) \\ -\delta \mathbf{u}_N^T\left[\int 3 K \mathbf{B}_V^T \Phi_P d V\right] \boldsymbol{\lambda}_e & -\delta \mathbf{u}_N^T\left[\int 2 G \mathbf{B}_D^T \mathbf{M} \Phi_P d V\right] \boldsymbol{\mu}_e \end{aligned}$$

and, by introducing the equivalent nodal loads  $\mathbf{q}_N$ ,

$$\begin{aligned} \int \mathbf{b}^T \delta \mathbf{u} d V+\int \mathbf{f}^T \delta \mathbf{u} d S & = \\ =\delta \mathbf{u}_N^T\left\{\int \Phi^T \mathbf{b} d V+\int \Phi^T \mathbf{f} d S\right\} & =\delta \mathbf{u}_N^T \mathbf{q}_N \quad (5b) \end{aligned}$$

Eventually, the usual assembly process will lead to the governing equation

$$\mathbf{K} \mathbf{U}-\mathbf{L}_V \boldsymbol{\lambda}-\mathbf{L}_D \boldsymbol{\mu}=\left[\mathbf{K}_V+\mathbf{K}_D\right] \mathbf{U}-\mathbf{L}_V \boldsymbol{\lambda}-\mathbf{L}_D \boldsymbol{\mu}=\mathbf{Q} \quad (6)$$

where  $\mathbf{u}$ ,  $\boldsymbol{\lambda}$ ,  $\boldsymbol{\mu}$  and  $\mathbf{Q}$  collect the subvectors  $\mathbf{u}_N$ ,  $\boldsymbol{\lambda}_e$ ,  $\boldsymbol{\mu}_e$  and  $\mathbf{q}_N$ , while the matrices  $\mathbf{K}_V$ ,  $\mathbf{K}_D$ ,  $\mathbf{L}_V$  and  $\mathbf{L}_D$  are obviously determined by considering the contributions given by the matrices obtained by solving the integrals on the right hand side of eqn. (5a). Of course, as clearly pointed out in eqn. (6),  $\mathbf{K}=\mathbf{K}_V+\mathbf{K}_D$ .

Eqn. (6) can also be written in incremental form:

$$\mathbf{K} \Delta \mathbf{U}-\mathbf{L}_V \Delta \boldsymbol{\lambda}-\mathbf{L}_D \Delta \boldsymbol{\mu}=\Delta \mathbf{Q} \quad (7)$$

At each time-step, a solution that satisfies both the governing equation and the constitutive law can be found by implementing an iterative procedure. In fact, for a given  $\Delta \mathbf{Q}$ , we can compute a vector  $\Delta \mathbf{U}=\Delta \mathbf{U}_1$  by solving eqn. (7) for  $\Delta \boldsymbol{\lambda}=\Delta \boldsymbol{\mu}=\mathbf{0}$ . At this stage, it is possible to set  $\Delta \boldsymbol{\lambda}=\Delta \boldsymbol{\lambda}_1$  and  $\Delta \boldsymbol{\mu}=\Delta \boldsymbol{\mu}_1$ , where  $\Delta \boldsymbol{\lambda}_1$  and  $\Delta \boldsymbol{\mu}_1$  denote the isotropic and deviatoric components of the plastic strain increments, which would satisfy the constitutive law at the selected *strain points* if the actual incremental displacements were  $\Delta \mathbf{U}_1$ . Given the updated vectors  $\Delta \boldsymbol{\lambda}=\Delta \boldsymbol{\lambda}_1$  and  $\Delta \boldsymbol{\mu}=\Delta \boldsymbol{\mu}_1$ , we can solve eqn. (7) again and find a new vector  $\Delta \mathbf{U}=\Delta \mathbf{U}_2$ .

As obvious, a convenient termination criterion is needed to stop the process: for instance, it is possible

to impose a proper threshold to the ratios  $a_1/b_1$  and  $a_2/b_2$ , where  $a_1=\left\{\Delta \boldsymbol{\lambda}_i-\Delta \boldsymbol{\lambda}_{i-1}\right\}^T\left\{\Delta \boldsymbol{\lambda}_i-\Delta \boldsymbol{\lambda}_{i-1}\right\}$ ,  $b_1=\Delta \boldsymbol{\lambda}_{i-1}^T \Delta \boldsymbol{\lambda}_{i-1}$ ,  $a_2=\left\{\Delta \boldsymbol{\mu}_i-\Delta \boldsymbol{\mu}_{i-1}\right\}^T\left\{\Delta \boldsymbol{\mu}_i-\Delta \boldsymbol{\mu}_{i-1}\right\}$ ,  $b_2=\Delta \boldsymbol{\mu}_{i-1}^T \Delta \boldsymbol{\mu}_{i-1}$ .

In view of eqn. (1), we can also apply the principle of virtual works by considering (for each element) the *viscous strains* and the relevant, compatible nodal displacements  $\hat{\mathbf{u}}_N$ . If we do so, we obtain

$$\begin{aligned} \int\left\{3 K^* \boldsymbol{\xi}_m+2 G^* \mathbf{d}+3 \eta_V \dot{\boldsymbol{\xi}}_m+2 \eta_D \dot{\mathbf{d}}\right\}^T\left\{\delta \boldsymbol{\xi}_m+\mathbf{M} \delta \mathbf{d}\right\} d V & = \\ =\delta \hat{\mathbf{u}}_N^T \mathbf{q}_N \quad (8) \end{aligned}$$

By setting, as before,  $\boldsymbol{\xi}_m=\mathbf{B}_V \hat{\mathbf{u}}_N$  and  $\mathbf{d}=\mathbf{B}_D \hat{\mathbf{u}}_N$ , an obvious assembly process will lead to the linear system  $\left[\mathbf{S}_V+\mathbf{S}_D\right] \hat{\mathbf{U}}+\left[\mathbf{H}_V+\mathbf{H}_D\right] \dot{\hat{\mathbf{U}}}=\mathbf{Q}$ .

In this equation,  $\hat{\mathbf{U}}$  collects all the nodal viscous displacements, while the entries of the matrices  $\mathbf{S}_V$ ,  $\mathbf{S}_D$ ,  $\mathbf{H}_V$  and  $\mathbf{H}_D$  can be determined by considering the contributions given by the integrals on the left hand side of eqn. (8). More precisely,  $\mathbf{S}_V$ ,  $\mathbf{S}_D$ ,  $\mathbf{H}_V$  and  $\mathbf{H}_D$  are concerned with the integrals characterized by the parameters  $K^*$ ,  $G^*$ ,  $\eta_V$  and  $\eta_D$ , respectively.

Now, we can compute the displacements due to viscosity by considering the following equation:

$$\begin{aligned} \left[\mathbf{S}_V+\mathbf{S}_D\right]\left\{\hat{\mathbf{U}}_0+\Delta \hat{\mathbf{U}}\left(t-t_0\right) / \Delta t\right\}+\left[\mathbf{H}_V+\mathbf{H}_D\right] \dot{\hat{\mathbf{U}}}(t) & = \\ =\mathbf{Q}_0+\Delta \mathbf{Q}\left(t-t_0\right) / \Delta t=\mathbf{K}\left\{\mathbf{U}_0+\Delta \mathbf{U}\left(t-t_0\right) / \Delta t\right\}+ \quad (9) \\ -\mathbf{L}_V\left\{\boldsymbol{\lambda}_0+\Delta \boldsymbol{\lambda}\left(t-t_0\right) / \Delta t\right\}-\mathbf{L}_D\left\{\boldsymbol{\mu}_0+\Delta \boldsymbol{\mu}\left(t-t_0\right) / \Delta t\right\} \end{aligned}$$

with  $t_0 \leq t \leq t_0+\Delta t$ .

In the above equation,  $\mathbf{U}_0$ ,  $\hat{\mathbf{U}}_0$ ,  $\mathbf{Q}_0$ ,  $\boldsymbol{\lambda}_0$  and  $\boldsymbol{\mu}_0$  denote (known) values attained at the beginning the current time-step (which is supposed to occur during the time interval  $\Delta t$ ), while  $\Delta \mathbf{U}$ ,  $\Delta \boldsymbol{\lambda}$  and  $\Delta \boldsymbol{\mu}$  are the increments that satisfy the governing equation (7) and the constitutive law. Clearly, the objective is to compute the (unknown) incremental vector  $\Delta \hat{\mathbf{U}}$ .

As suggested by eqn. (9), it is reasonable to assume a linear variation of  $\Delta \mathbf{U}$ ,  $\Delta \hat{\mathbf{U}}$ ,  $\Delta \boldsymbol{\lambda}$  and  $\Delta \boldsymbol{\mu}$  during the current time-step. In consequence, the relevant velocity  $\dot{\hat{\mathbf{U}}}(t)$  shall be constant. Therefore, we can set  $\dot{\hat{\mathbf{U}}}=\Delta \hat{\mathbf{U}} / \Delta t$  and satisfy eqn. (9) at the time  $t=t_0+\Delta t / 2$ , when the terms which depend on  $\Delta \mathbf{U}$ ,  $\Delta \hat{\mathbf{U}}$ ,  $\Delta \boldsymbol{\lambda}$  and  $\Delta \boldsymbol{\mu}$  attain their mean values. This implies the solution of the linear system

$$\begin{aligned} \left[\mathbf{S}_V+\mathbf{S}_D\right]\left\{\hat{\mathbf{U}}_0+\frac{1}{2} \Delta \hat{\mathbf{U}}\right\}+\left[\mathbf{H}_V+\mathbf{H}_D\right] \Delta \hat{\mathbf{U}} / \Delta t & = \\ =\mathbf{K}\left\{\mathbf{U}_0+\frac{1}{2} \Delta \mathbf{U}\right\}-\mathbf{L}_V\left\{\boldsymbol{\lambda}_0+\frac{1}{2} \Delta \boldsymbol{\lambda}\right\}-\mathbf{L}_D\left\{\boldsymbol{\mu}_0+\frac{1}{2} \Delta \boldsymbol{\mu}\right\} \quad (11) \end{aligned}$$

in which the only unknown is the vector  $\Delta \hat{\mathbf{U}}$ .

### III. NUMERICAL TESTS

The material model discussed in the previous Section, implemented in a finite element code, was applied to the analysis of a test specimen with the aim of comparing some numerical and experimental results. Namely, we considered a cylindrical specimen subjected to a uniformly distributed compression

force, first by performing a *static creep test*, next by imposing a repeated *square-wave load*. The thickness of the specimen was 130 mm and its radius 50 mm.

As for the plastic strains, we only focused on time-dependent increments, assuming that they could simply be proportional to the reversible strains through a dimensional coefficient  $\beta$ .

In order to do so, we simply set  $\Delta \epsilon^p = \beta (\epsilon_m - \epsilon^p) \Delta t$  and  $\Delta e^p = \beta (e - e^p) \Delta t$ , adding the condition that the plastic strain increments (at any *strain point*) could be non-zero only when the parameter  $\rho = \{\mathbf{e} + \mathbf{d}\}^T \mathbf{M} \{\mathbf{e} + \mathbf{d}\}$  turned out to be higher than any previous value.

Incidentally, it may be worth noting that a more general model should include viscous strains, instantaneous elastic (reversible) and plastic (non-reversible) strains, as well as time-dependent elastic and plastic strains. Instead, for the sample problems discussed below, we did not take into account instantaneous plastic strains.

Thanks to the geometry of the test specimen and to the presence of planes of symmetry, it was possible to discretize just a small portion of the specimen, by using six 15-node pentahedral elements and twelve 20-node hexahedral elements with a total number of 128 nodes.

With reference to Fig. 1a, we focused on the top portion schematically represented in grey and the required loads were applied to the upper surface in the model shown in Fig. 1b. In addition,  $x$ -displacements,  $y$ -displacements and  $z$ -displacements were set equal to zero for all the nodes belonging to the planes  $x=0$ ,  $y=0$ , and  $z=0$ , respectively.

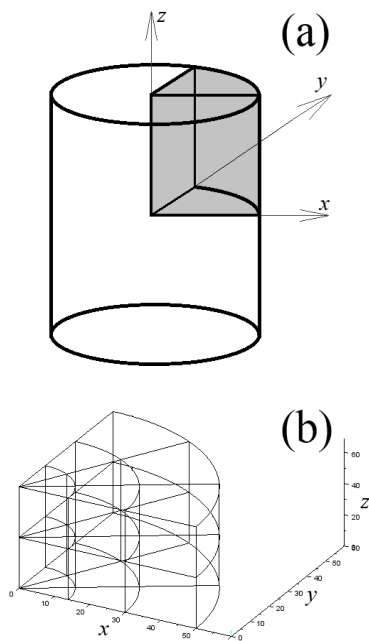


Fig. 2. Test specimen and discrete model.

The first numerical tests were concerned with the *square-wave repeated load*, since an initial, reasonable estimate of the parameters was possible by means of a simple *trial and error procedure*. Of

course, it would have been possible to obtain better results through a different approach, such as the one, which will be briefly discussed later with reference to *static creep tests*.

In the case of *square-wave loading*, the influence of different values of the parameters can be immediately appreciated, as shown (for instance) by the graphs in Fig. 3, where we focused on the role played by the elastic moduli  $E$  and  $E^*$ .

Thus, for a given load sequence, we compared an initial solution obtained with  $E=1100$  MPa,  $E^*=250$  MPa,  $\eta_v=500$  MPa s,  $\eta_D=5000$  MPa s and  $\beta=0.0053$  s<sup>-1</sup> with the solutions given by changing  $E$  (set equal to 1300 MPa) and  $E^*$  (set equal to 230 MPa).

Note that Poisson's ratio was assumed to be equal to 0.35 both for the contribution given to the instantaneous elastic response and for the contribution given to the viscoelastic response.

As for the *square-wave load*, we made use of a load sequence measured during an actual test, when eighty cycles were applied by imposing compression surface forces that attained the value of about 0.1 MPa in 0.015 s, remained nearly constant for 0.51 s, dropped to about 0.005 MPa in 0.015 s and remained nearly constant for 0.46 s.

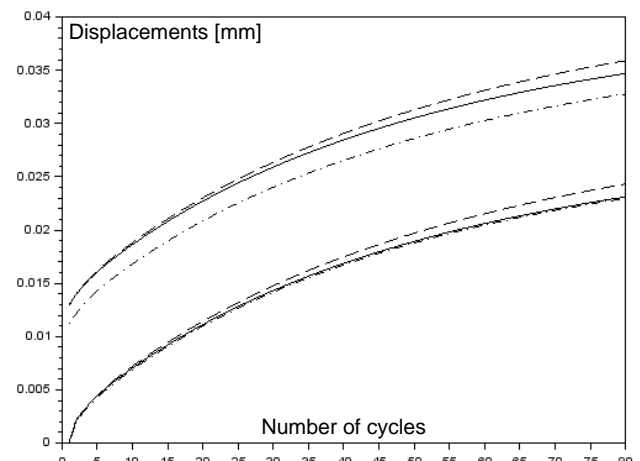


Fig. 3. Initial solution (solid line) compared with the solutions given by  $E=1300$  MPa (dash-dotted line) and  $E^*=230$  MPa (dashed line).

As shown in Fig. 3, higher values of  $E$  tend to reduce the largest relative displacements, while lower values of  $E^*$  tend to increase both the largest and the smallest relative displacements. It can also be noted that the minimum values are hardly affected by the choice of  $E$ , since the lower solid and dash-dotted lines are practically coincident.

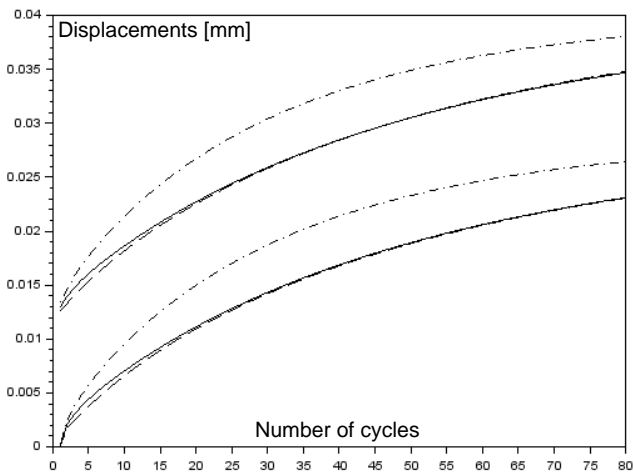


Fig. 4. Initial solution (solid line) compared with the solutions given by  $\eta_D=3000 \text{ s}^{-1}$  (dash-dotted line) and  $\eta_V=2000 \text{ s}^{-1}$  (dashed line).

Next, we focused on different values of the viscous parameters:  $\eta_V=2000 \text{ MPa s}$  and  $\eta_D=3000 \text{ MPa s}$ . In spite of its significant increment,  $\eta_V$  only had minor consequences on the first part of the curves, as shown in Fig. 4, where the solid and dashed lines are mostly superimposed.

Instead, lower values of  $\eta_D$  had the effect to increase both the largest and the smallest relative displacements. In practice,  $\eta_D$  and  $E^*$  behave in a similar way, but there seems to be an interesting difference: lower values of  $\eta_D$  tend to decrease the radius of curvature of the plots, while lower values of  $E^*$  tend to increase it.

We also made a test to check the influence of the parameter  $\beta$ , but we found that its role was negligible, since a percentage difference greater than 20% ( $\beta=0.004 \text{ s}^{-1}$ ) practically gave the same response in terms of minimum/maximum values.

Next, as already pointed out, we focus on experimental data obtained by considering a cylindrical specimen (130 mm thick with a 50 mm radius). The first test was carried out by imposing a periodic load characterized by the already mentioned square-wave pattern (with a compressive surface force ranging between 0.005 and 0.1 MPa). Measurements were taken every 0.001 s and the same time interval was used for the numerical analysis.

The second test (a static creep test) involved a compressive surface force, which attained the value 0.1 MPa in 4 s, decreased to 0.042 in 10 s and remained nearly constant for 2 s. In this case, measurements were taken every 0.01 s and the same time interval was used for the numerical analysis. On this occasion, we aimed at estimating parameters that could provide numerical results similar to the measured data that had been collected in both tests. Of course, we had to look for a compromise solution, since the model is relatively simple and cannot be

expected to accurately describe any aspect of complex phenomena.

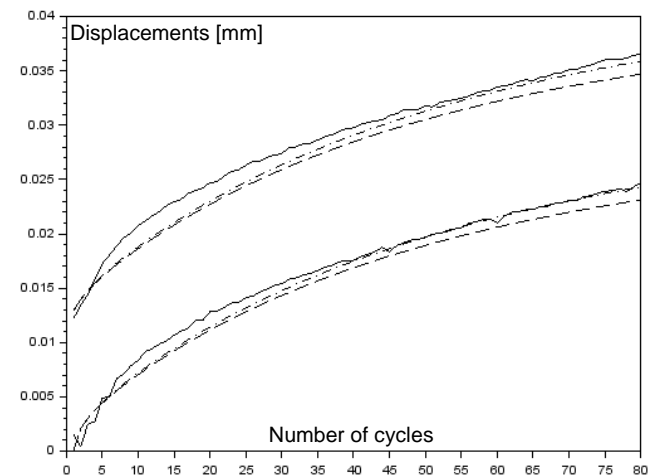


Fig. 5. Square-wave repeated load: comparison between numerical results and experimental data (black solid line).

Thus, after checking the influence of each parameter on both sample cases, we ended up with  $E=1100 \text{ MPa}$ ,  $\eta_V=500 \text{ MPa s}$ ,  $\eta_D=5000 \text{ MPa s}$  and two possible sets of values for  $E^*$  and  $\beta$ :  $E^*=250 \text{ MPa}$ ,  $\beta=0.0053 \text{ s}^{-1}$  and  $E^*=230 \text{ MPa}$ ,  $\beta=0.0049 \text{ s}^{-1}$ .

The effects of these choices can be visually appreciated by examining the plots in Figs. 5 and 6, where the black solid lines are concerned with the experimental data (minimum and maximum values of the relative displacements during eighty cycles for the square-wave loading, relative displacements between the top and bottom surface of the cylindrical specimen for the static creep test).

On the contrary, the dashed and dash-dotted lines correspond to the numerical responses obtained with  $E^*=250 \text{ MPa}$ ,  $\beta=0.0053 \text{ s}^{-1}$  and  $E^*=230 \text{ MPa}$ ,  $\beta=0.0049 \text{ s}^{-1}$ , respectively.

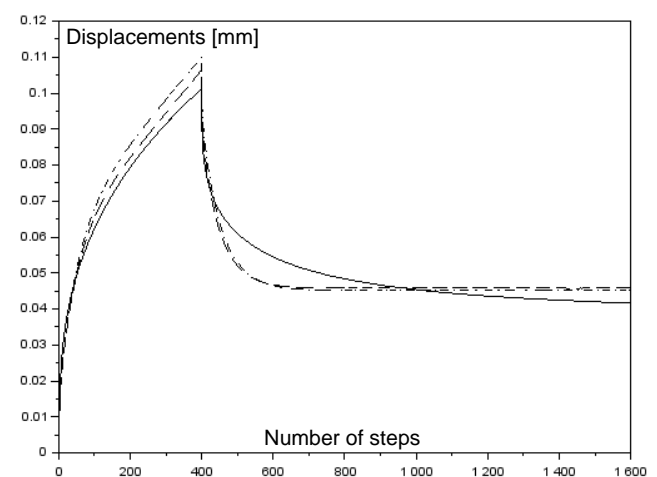


Fig. 6. Static creep test: comparison between numerical results and experimental data (black solid line).

Clearly, the values  $E^*=230 \text{ MPa}$  and  $\beta=0.0049 \text{ s}^{-1}$  represent a better solution for the square-wave loading, but imply a worse approximation for the static creep test.

As obvious, when we wish to focus on the level of accuracy, it is convenient to make use of an objective *error indicator*.

To this aim, we introduced the parameter  $\zeta = \sqrt{r}$  with  $r = (\mathbf{c} - \mathbf{m})^T (\mathbf{c} - \mathbf{m}) / (\mathbf{m}^T \mathbf{m})$ , if  $\mathbf{c}$  and  $\mathbf{m}$  are vectors of the computed and measured values. More precisely, in this context, they must represent the minimum and maximum values related to each pair of plots in Fig. 5 or the values needed for every plot in Fig. 6.

Eventually, with reference to Fig. 5, we obtained  $\zeta = 0.05618$  and  $\zeta = 0.0369$  when we considered the results that correspond to the dashed and dash-dotted line, respectively.

Instead, with reference to Fig. 6, we obtained  $\zeta = 0.0696$  for the numerical solution concerned with the dashed line and  $\zeta = 0.0812$  for the results related to the dash-dotted line.

In other words, when we try to improve the accuracy of the numerical analysis related to the *square-wave loading*, we obtain worse results for the simulation of the *static creep test* and viceversa.

This fact can be investigated further by looking for an optimal solution concerned with the *static creep test* and checking what happens if we try to simulate the *square-wave loading* case by using the same parameters.

We actually estimated the optimal values of  $E^*$ ,  $\eta_V$ ,  $\eta_D$  and  $\beta$  by considering the experimental results of the *static creep test*, by assuming  $E = 1100$  MPa (*i.e.*, the elastic modulus needed to obtain a correct difference between the maximum and minimum displacements with *the square-wave load*) and by setting Poisson's ratios equal to 0.35.

For the estimate, we essentially made use of an iterative algorithm discussed in a previous work [6], which can be briefly describes as follows:

1. For a given set of initial parameters, we started to adjust the value of  $E^*$  with the aim of reducing the error indicator  $\zeta$ ; in order to do so, we considered an increment  $\Delta_1 = E^*/2^7 > 0$  and kept increasing  $E^*$  if  $\zeta$  continued to decrease; similarly, if/when a greater value of  $\zeta$  was found, a new increment  $\Delta_2 = -\Delta_1/2 < 0$  was considered; next, we set  $\Delta_3 = -\Delta_2/2 > 0$ , if/when  $\zeta$  began to increase, and so on; we stopped the process when the absolute value of the increment was less than the initial value of  $E^*$  divided by 1,000 or when the absolute value of the difference between the last and the initial value of  $E^*$  was greater than the initial value of  $E^*$  divided by 10
2. We did the same with the parameters  $\eta_D$ ,  $\eta_V$  and  $\beta$ ; of course, during each phase of this process (*i.e.*, while updating each parameter), we made use of the previous estimates of the other parameters
3. After updating all the parameters for the first time, we defined an *error indicator*, say  $\zeta_1$ , in order to

- quantify the improvement due to this phase of the process
4. We continued to update the same parameters by following the procedure describe above: each time, the initial value of every parameter to be modified was its last estimate; after estimating the fourth parameter, we also defined an *error indicator*  $\zeta_k$ , with  $k=2,3,4,\dots$
5. The process continued until the ratio  $(\zeta_{k-1} - \zeta_k) / \zeta_{k-1}$  was less than 0.0001

We applied this procedure by considering (as initial values) the parameters that had been determined through a *trial and error process* and had implied the lower difference between the *error indicators* concerned with the *square-wave loading* and the *static creep test*. Thus, we set  $E^* = 250$  MPa,  $\eta_V = 500$  MPa s,  $\eta_D = 5000$  MPa s and  $\beta = 0.0053$  s<sup>-1</sup>. Actually, in view of the plots corresponding to the dashed lines in Figs. 5 and 6 (characterized by  $\zeta = 0.05618$  and  $\zeta = 0.0696$ , respectively), these parameters seemed to represent a sort of *fair compromise*.

At the end of the parameter estimation procedure, we obtained the values  $E^* = 248.23$  MPa,  $\eta_V = 419.62$  MPa s,  $\eta_D = 6730.72$  MPa s and  $\beta = 0.00520811$  s<sup>-1</sup>. The relevant *error indicator* turned out to be 0.0574.

As shown in Fig. 7, the numerical response (dashed line) appears to represent a significant improvement (which can be clearly noticed), if we compare the relevant graph with the plots of Fig. 6. However (as obviously expected), the estimated parameters imply a poor performance, if they are utilized with the aim of simulating the *static creep test*.

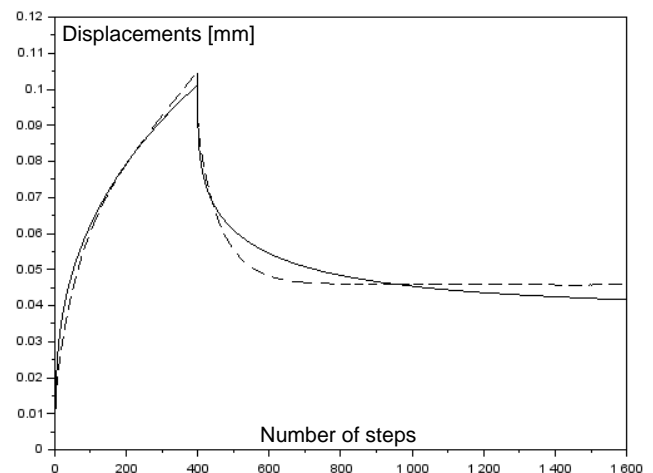


Fig. 7. *Static creep test: comparison between the experimental data (black solid line) and the optimal solution.*

As a matter of fact, the response in terms of minimum/maximum displacements per cycle is reported in Fig. 8 with dashed lines and there appears to be an impressive difference with respect to the experimental data. Naturally, the extremely crude approximation is reflected by the value attained by the *error indicator*:  $\zeta = 0.1443$ .

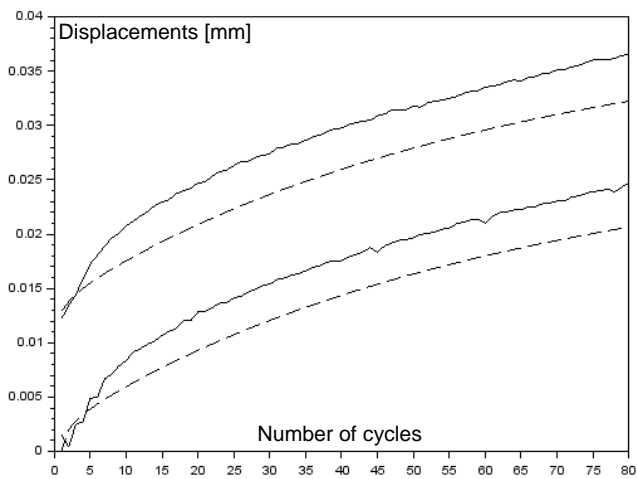


Fig. 8. Square-wave repeated load: comparison between the experimental data (black solid line) and the numerical results obtained by using the parameters that provide an optimal solution for the static creep tests.

Surely, it is worth noting that a *slightly better compromise* could be achieved by implementing a proper algorithm, which is aimed at estimating parameters that simultaneously minimize the difference between the *error indicators* concerned with the *square-wave loading* and the *static creep test*.

However, the overall gain would certainly be rather poor, as suggested by the dash-dotted line in Fig. 6: in consequence of the improvement for the *square-wave loading* profile ( $\zeta=0.0369$  instead of  $\zeta=0.05618$  with  $E^*=230$  MPa in place of  $E^*=250$  MPa), we ended up with a definitely worse approximation for the *static creep test* ( $\zeta=0.0812$  instead of  $\zeta=0.0696$ ).

Similarly, the optimal solution concerned with Fig. 7 and the very bad results reported in Fig. 8, make it clear that a significant improvement of the numerical simulation of the *static creep test* can only lead to a poor performance when the *square-wave load* comes into play.

#### IV CLOSING REMARKS

The aim of this paper was a preliminary study (based on a comparison with experimental data) to investigate the potential of a *viscoelastic-plastic material model*, which is relatively simple, can be used with three-dimensional stress states and makes a clear distinction between deviatoric strains and volumetric strains.

Since the research activity was carried out with the objective of giving a contribution in the field of pavement design, the experimental data were concerned with a cylindrical specimen which was made of a *bituminous mixture*. The relevant measurements were taken by considering a *static creep test* and a *square-wave load*. In this way, it was possible to check if the proposed model was actually able to describe the material response to different load conditions and, in consequence, could serve as a valuable alternative to more traditional elastic models, which can definitely be employed to assess the

strength of a structure, but are obviously not adequate to simulate time-dependent phenomena.

The numerical examples reported here confirm the results of a previous work [6], which showed that the model could describe time-dependent phenomena related to creep and pulse loads in an adequate way.

Of course, it should be noticed that the model is relatively simple, requires a limited number of parameters and (in the present form) can only be used for macroscopically homogeneous materials. This means that we cannot expect to estimate a set of parameters, which provide excellent accuracy for any type of load condition.

In consequence, even though it seems possible to define parameters which provide an optimal response for a specific load sequence, in general a *compromise solution* seems to be the best choice for general applications.

In actual fact, the numerical results discussed in the previous Section show that the experimental measures concerned with a *static creep test* and a *square-wave load* can be approximated with a satisfactory level of accuracy by means of a convenient choice of the parameters.

Therefore, it seems reasonable to claim that the model presented in this paper can be considered in any situation in which we are interested in studying the basic behavior of *bituminous mixture* in the presence of time-dependent load conditions. It is also worth noting that the proposed nonlinear analysis only requires a moderate computational effort and that time-dependent effects cannot be evaluated at all by assuming a more traditional and more elementary elastic material model.

Finally, it is quite obvious that a more sophisticated model could be developed, with the aim of introducing elements which come into play in the presence of quasi-static loads and elements which only have an effect when time-dependent loads are considered. If we do so, more accurate results are to be expected for different load conditions.

#### REFERENCES

- [1] P.M. Naghdi, S.A. Murch, "On the Mechanical Behavior of Viscoelastic/Plastic Solids", *Journal of Applied Mechanics*, 30(3), 321-328, 1963.
- [2] R.A. Schapery, "On the characterization of nonlinear viscoelastic materials", *Polymer Engineering and Science*, 9(4), 295-310, 1969.
- [3] J. Menčík, G. Rauchs, J. Bardon, A. Riche, "Determination of elastic modulus and hardness of viscoelastic-plastic materials by instrumented indentation under harmonic load", *Journal of Materials Research*, 20, 2660–2669, 2005.
- [4] H. Kruggel-Emden, S. Wirtz, V. Scherer, "A study on tangential force laws applicable to the

discrete element method (DEM) for materials with viscoelastic or plastic behavior”, *Chemical Engineering Science*, 63(6), 1523-1541, 2008.

[5] R.F. Cook, “A flexible model for instrumented indentation of viscoelastic–plastic materials”, *MRS Communications*, 8, 586–590, 2018

[6] B. Crisman, A. Nappi, “Viscoelastic-plastic Materials: Parameter Estimate and Numerical Simulation of Experimental Tests”, *Journal of Multidisciplinary Engineering Science and Technology (JMEST)*, 6(11), 11056-11067, 2019.

[7] J. Neves, A. Gomes-Correia, “Evaluation of the stiffness modulus of bituminous mixtures using laboratory tests (NAT) validate by field back-analysis”, in *Proceedings Seventh International Conference on the Bearing Capacity of Roads, Railways and Airfields* (edited by I. Horvli), 7th BCRRA Conference, Trondheim, Norway 25 - 27 June 2005.

[8] M.R. Taha, S. Hardwiyono, N.I.Md. Yusoff, M.R. Hainin, J. Wu, K.A.M. Nayan, “Study of the Effect of Temperature Changes on the Elastic Modulus of Flexible Pavement Layers”, *Research Journal of Applied Sciences, Engineering and Technology*, 5(5), 1661-1667, 2013.

[9] A. Setiawan, L.B. Suparma, A.T. Mulyono, “Developing the Elastic Modulus Measurement of Asphalt Concrete Using the Compressive Strength Test”, in *AIP Conference Proceedings* 1855, 2017.